Fizika Nizkikh Temperatur, 2008, v. 34, Nos. 4/5, p. 496–503

Electron attachment to atomic hydrogen on the surface of liquid ^{4}He

Toshikazu Arai

Research Center for Low Temperature and Materials Sciences, Kyoto University, Kitashirakawa-Oiwake-cho, Sakyo-ku, Kyoto, 606-8502, Japan
E-mail: toshikaz@scphys.kyoto-u.ac.jp

Hideki Yayama

Department of Physics, Kyushu University, 4-2-1 Ropponmatsu, Chuo-ku, Fukuoka, 810-8560, Japan

Kimitoshi Kono

RIKEN, Low Temperature Physics Laboratory, Hirosawa 2-1, Wako-shi, Saitama, 351-0198, Japan

Received November 6, 2007

We demonstrate a possibility that helium surface electrons at cryogenic temperatures can be used as a new source of very low energy electrons. Since both electrons (e^-) and hydrogen atoms (H) are bound on liquid helium surface, two-dimensional mixture gas of these two species is available on the surface. We found that low energy collision of e^- and H drives electron attachment to form a negative hydrogen ion (H^-) in the mixture. From our temperature dependence measurement of the reaction rate, it was found that another H atom participate in the reaction. Namely, the reaction is expressed as $H + H + e^- \rightarrow H^- + H$. Possible reaction mechanisms are discussed in terms of direct three-body process and dissociative attachment process. Measurements in applied magnetic field (B) show that the reaction rate coefficient is suppressed as $\sim B^{-2}$. This implies that electron spin singlet collision is relevant for electron attachment.

PACS: 67.63.Gh Atomic hydrogen and isotopes;
67.25.–k ^{4}He;
68.03–g Gas-liquid and vacuum-liquid interfaces.

Keywords: surface state electrons, atomic hydrogen, electron attachment.

Introduction

Slow electron impact on atoms and molecules is a general phenomenon that plays an important role in interstellar chemical reactions, ionosphere processes, discharge, and so forth [1]. Also, it has been reported that slow electron collisions may induce substantial damages in DNA strands and other biomolecules [2]. Slow electron scattering phenomena have been studied mainly using electron beams. In spite of the recent progress of experimental techniques, spectroscopy at electron energies much less than 100 meV with resolutions better than 5 meV is still difficult [1]. Therefore, phenomena occurring in dark nebulae, for example, where the temperature is approximately 10 K ($\approx$ 1 meV), are experimentally inaccessible. In order to study such phenomena, much slower incident electrons are required.

When electrons (e^-) are subjected to cryogenic environment and they are in equilibrium with surrounding temperature, we may acquire very low energy electron source. By using a modern dilution refrigerator, temperature range as low as 10 mK is an easy access. Thermal kinetic energy of electrons at 10 mK is less than 0.001 meV. By varying temperature, the electron energy is tunable.

Electrons outside but very close to the surface of liquid helium at cryogenic temperature is known to form bound states in the attractive image potential [3]. The motion of those electrons perpendicular to the surface is restricted, whereas their motion along the surface is nearly free. Collection of helium surface state electrons (SSE) are then interpreted as a two-dimensional (2D) gas and it is ther-

mally in equilibrium with the underlying liquid helium. The properties of SSE are well understood [4]. We demonstrate here that SSE can be used as a source of very low energy electrons.

As a collision target, we employ atomic hydrogen (H) in this work. Properties of H gas at low temperature has been extensively studied, motivated by the interest that cold H gas behaves as a quantum gas [5,6]. Since H atom is a Boson, cold H gas exhibits quantum phase transitions such as Bose–Einstein condensation in three dimensions [7] and Kosterlitz-Thouless transition in two dimensions [8]. For the stabilization of H gas at low temperatures, it is crucial to minimize recombination rate of the atoms into H_2 molecules. In order to avoid rapid recombination of adsorbed H atoms on the sample cell walls, wall coating by superfluid helium film is necessary. Binding energy of a H atom on superfluid ^{4}He surface is 1.0 K and it is orders of magnitude smaller than metal or other solid surfaces. Superfluid wall coating was originally developed by Silvera and Walraven [9], and it is now a standard technique for cryogenic H experiments.

H atoms in a wall-coated sample cell are in equilibrium between bulk gas phase and surface adsorbed phase. Adsorbed H atoms behave like 2D gas as well as SSE. Since either electrons and H atoms are bound on liquid helium surface, we are able to mix them and study the phenomena driven by low energy e^-–H collisions.

Our preliminary measurements showed that a chemical reaction of e^- with H takes place on the surface and gives rise to a reduction of SSE density at temperature-dependent rates [10–12].

In this paper, we show that the reaction involves two H atoms and one electron, namely, $H + H + e^- \rightarrow H^- + H$. On the basis of this result, we discuss two possible reaction mechanisms: direct three-body process and dissociative attachment process.

Apparatus

In this section, we show our apparatus for the reaction rate measurement of e^- and H in 2D mixture gas on liquid helium surface.

We used a dilution refrigerator to obtain low temperatures. Our apparatus consists of a sample cell on the mixing chamber, a H_2 dissociator and a 0–12 T superconducting magnet for the magnetic field dependence measurement. The H_2 dissociator is thermally anchored on the still in the zero-field measurement and on the mixing chamber in the magnetic field dependence measurement.

SSE is prepared in the sample cell and H atoms are created in the dissociator. H atoms are guided to the sample cell through a capillary. H atoms in the sample cell are partly adsorbed on the liquid helium covered surface and mixed with SSE.

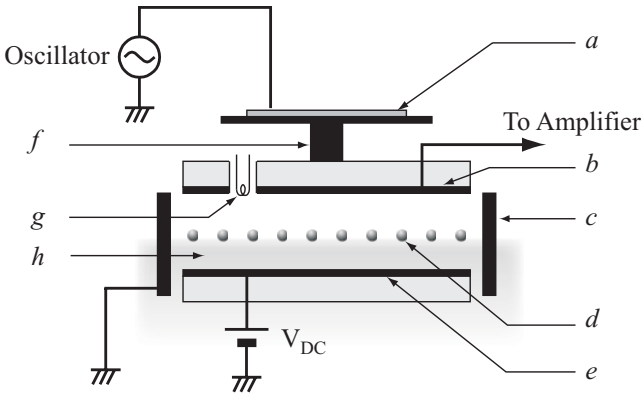

Fig. 1. Arrangement of the electrodes in the experimental cell: piezo actuator (*a*), upper electrode (*b*), guard ring (*c*), SSE (*d*), lower electrode (*e*), mechanical connection (*f*) of (*a*) and (*b*), tungsten filament (*g*),liquid ^{4}He (*h*).

The sample cell contains a filament as an electron source, an assembly of electrodes for SSE confinement and a vibration capacitor electrode (VCE) for surface charge measurement. The sample cell is 44 mm inner diameter and 30 mm depth copper cylinder. Electrodes are arranged as illustrated in Fig. 1. The upper and lower electrodes are parallel disks made from copper plated glass-epoxy printed circuit board, 25 mm in diameter and 3 mm appart. The cell is partly filled with liquid ^{4}He. The liquid level, which is precisely known from the capacitance, is set 1 mm above the lower electrode.

A tungsten filament at a tiny hole of the upper electrode is briefly heated to emit thermoelectrons. It is operated at 1.5 K where good amount of helium vapor exists to slow down the hot electrons by collisions before they reach the surface. It is required to heat the filament while H atoms are absent in the cell, otherwise the heat burns off the superfluid film on the filament and all H atoms rapidly recombine on the bare surface.

A positive DC potential, V_{DC}, is applied to the lower electrode while the potentials of the upper electrode and the guard ring are ground level. The electric field between upper and lower electrodes presses SSE to the surface. The guard ring produces a radial confinement potential for SSE.

Total amount of surface charge is measured by employing VCE [11]. Our VCE consists of the upper electrode which is mechanically connected to, but electrically isolated from, the piezo actuator and the positively biased lower electrode. SSE layer screens the electric field between the electrodes in proportion to the SSE density σ_e. The piezo actuator drives an vibration of the upper electrode. The vibration in the electric field induces an AC current to the upper electrode. The current amplitude I is given by

$$I = \frac{A_e a\omega}{d^2}(-b\sigma_e e + \varepsilon_0 V_{DC}). \quad (1)$$

Here, A_e is the area of an electrode disk, ω is the angular frequency, d is the separation of the electrodes, b is the distance of the SSE layer from the lower electrode, $-e$ is the electronic charge and ε_0 is permittivity of vacuum. The relative dielectric constant of liquid helium is approximated to unity. From Eq. (1), we see that VCE is sensitive at large a and ω. We operate our VCE at a and ω as large as possible on conditions that its linearity is maintained and heating of the cell is negligible. An aquadag film bolometer [13] in the cell allows us to sense the heating. In this experiment $V_{DC} = 90$ V. VCE is operated at $\omega/2\pi = 880$ Hz and the driving voltage of the piezo actuator 5.0 V peak-to-peak. We estimate that $a = 76$ nm from measured I for $\sigma_e = 0$. Since $I \geq 0$, σ_e is necessarily smaller than saturation density $\sigma_e^{\text{sat}} (= \varepsilon_0 V_{DC}/be)$. σ_e^{sat} is the maximum SSE density and it is $5.0 \cdot 10^8$ electrons/cm^2 for our conditions. The VCE resolution is $2 \cdot 10^5$ electrons/cm^2 which is 0.04% of σ_e^{sat}.

Figure 2 shows the diagram of electronics for VCE measurement. Dry batteries supply V_{DC}. The signal current is measured by a current-to-voltage preamplifier (Stanford Research Systems, Model 570). The upper electrode is virtually grounded in this preamplifier. Unwanted signals from direct capacitive coupling of the upper electrode with the piezo actuator and with the lower electrode are canceled by employing a phase shifter, an attenuator and a differential amplifier (NF corporation, 5305). VCE is calibrated as follows. First, we take the signal at $\sigma_e = 0$ and $V_{DC} = 0$. This signal corresponds to $\sigma_e = \sigma_e^{\text{sat}}$ at given V_{DC}. Next, we apply V_{DC} and measure the signal at $\sigma_e = 0$. The signal at finite σ_e at applied V_{DC} moves between these two points as a linear function of σ_e.

Hydrogen atoms are created in a cryogenic H_2 dissociator. A helical resonator [14] in the dissociator is excited by rf pulses to ignite glow discharge of helium vapor. It is supposed that the charged particles hit and dissociate the frozen H_2 molecules at the wall. This technique was originally developed by Hardy *et al.* [15] and we referred to van Roijen *et al.* [16] to design our dissociator.

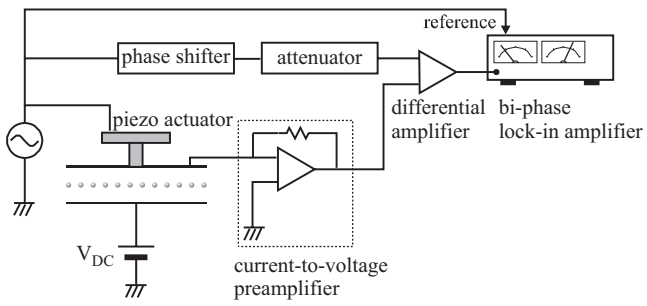

Fig. 2. Diagram of the detection electronics.

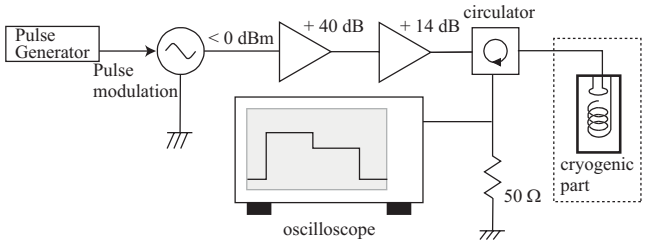

Fig. 3. Electronics for cryogenic pulsed rf discharge hydrogen dissociation.

Figure 3 is a diagram of rf discharge electronics. The pulse generator generates 100 μs pulses and it activates the rf synthesizer (Anritsu MG3642A) output during the pulse. We tuned the helical resonator to 430 MHz so that we are able to use less expensive amateur radio power amplifiers. The power amplifiers are purchased from Tokyo Hy-Power. The first one (PRA-15-430, custom made) amplifies 40 dB and the second one (HL-250 DX) 14 dB. Maximum available power is 54 dBm (250 W) at 0.0 dBm synthesizer output. High power pulses are only required for the first ignition after cooling. Once the discharge occurs, much smaller power is enough to start discharge from the second ignition. We suppose that is because charged particles live long in the dissociator. For the measurements described below, the synthesizer output is reduced to –9.0 dBm. The circulator (Tokyo Hy-Power A8713, custom made) is necessary to protect the amplifier from reflected waves. The reflected waves are terminated by a 50 Ω terminator. Discharge ignition can be recognized from sudden change of the reflected wave amplitude as it is shown on the screen of the oscilloscope in Fig. 3.

H atoms thus created are guided to the sample cell through a capillary tube. Discharge conditions, such as rf power, pulse width, number of pulses, pulse repetition rate and temperature of the dissociator, are carefully maintained so as to regulate the amount of H atoms fed to the cell. Discharge is operated after SSE containing experimental cell is cooled from 1.5 K down to working temperature.

Zero magnetic field measurements

We describe our measurements in the absence of applied magnetic field in this section.

As mentioned in the previous section, it is necessary to fill H atoms in the sample cell after SSE is prepared. We recorded VCE output before and after H atoms were filled. As a fixed amount of H atoms are fed into the cell, the VCE output starts to vary, signaling the loss of SSE. The influence of the H atoms is to diminish SSE from the surface. We confirmed that without H_2 stored in the dissociator, the discharge had no influence on the SSE

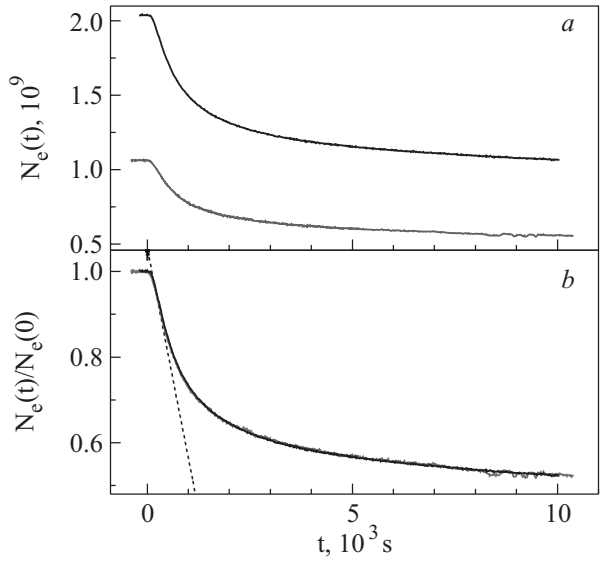

Fig. 4. Density decay curves of SSE ($T = 0.30$ K, $V_{DC} = 90$ V). Hydrogen atoms are fed at $t = 0$. These curves are measured under the same conditions except that the initial SSE densities are different (*a*). Two curves in (*a*) are normalized by the value at $t = 0$. Perfect scaling behavior is observed. (There are actually two lines overlapping each other.) The dotted line is the tangent at $t = 0$, which defines v_0 (*b*).

density. This means that atomic hydrogen does influence the SSE. Typical traces of the VCE output are shown in Fig. 4,*a*. Here, the vertical axis is the number of SSE (N_e) which is converted from the VCE output. At $t = 0$, H atoms are fed into the cell. Compared to the characteristic time ($\sim 10^3$ s) of SSE loss curve, a few seconds filling time of H atoms is short and we neglect it in the analysis. After H atoms are filled, the dissociator is switched off. The shown data were measured at T = 0.30 K and V_{DC} = = 90 V. Between the two curves only the initial number of SSE, $N_e(0)$ is different.

We attribute the SSE loss to the attachment of electrons to H atoms to form negative hydrogen (H^-) ions. The reaction product H^- must leave the surface since we measured the loss of surface charge by VCE. It is less probable for charges to escape from the surface into the free volume, because there is a potential barrier comparable to eV_{DC} that needs to be overcome. Then, the ions penetrate into the underlying liquid helium. The electrostatic energy gain may dominate over the loss due to the zero-point motion of the ion inside liquid He, which is essential for the electron bubble to form.

Here we would like to determine the reaction rate equation from the experiment. In general, one electron can react with n H atoms to form negative hydrogen, for which the chemical reaction formula is written as $e^- + nH \to H^- + (n-1)H$. This reaction occurs only in area A_e of lower electrode, where SSE are confined. Another relevant reaction that should be taken into account is the recombination of H atoms to form H_2 molecule: $H + H \to H_2$. H atoms exist on the entire surface area A of the cell with surface density σ_H as well as in the free volume V with volume density n_H [6]. The recombination occurs both on the surface and in the volume.

The rate equations for the total number of SSE, $N_e = A_e\sigma_e$, and of hydrogen atoms, $N_H = A\sigma_H + Vn_H$, may be written as

$$\frac{dN_e}{dt} = -K_e N_e(\alpha N_H)^n, \tag{2}$$

$$\frac{dN_H}{dt} = -K_e N_e(\alpha N_H)^n - K_s^{\text{eff}}(\alpha N_H)^2, \tag{3}$$

$$\alpha = [A + (V/\lambda_{th})e^{-E_a/k_BT}]^{-1}. \tag{4}$$

Here, K_e and K_s^{eff} are the rate coefficients for electron attachment and H–H recombination, respectively. We assumed the adsorption isotherm of H, $\sigma_H = n_H\lambda_{th} \times$ $\times \exp(E_a/k_BT)$, with the surface binding energy E_a and the thermal de Broglie wavelength $\lambda_{th} = (2\pi\hbar^2/m_Hk_BT)^{1/2}$, where m_H is the atomic hydrogen mass. We used the most reliable experimental value of E_a, 1.0 k_B [17], in the analysis. The coefficient α relates σ_H and N_H. Substitution of n_H in the N_H expression by the adsorption isotherm leads $\sigma_H = \alpha N_H$. The effective recombination rate coefficient K_s^{eff} is expressed in terms of surface and volume recombination rate coefficients, K_s and K_v, as $K_s^{\text{eff}} = AK_s + VK_v\lambda_{th}^{-2}\exp(-2E_a/k_BT)$ [6].

One of the most prominent properties of the observed SSE loss curves $N_e(t)$ is that when the loss curves are normalized by the initial number of SSE $N_e(0)$, all the curves with different $N_e(0)$ fall on a single curve (Fig. 4,*b*). This property implies that $d(\log N_e)/dt$ must be independent of N_e, and accordingly the evolution of $N_H(t)$ should be independent of N_e. This condition is satisfied if the first term in Eq. (3) is negligible in comparison with the second term, that is, the loss rate of H atoms is dominated by recombination rather than electron attachment.

The characteristic measure of the SSE loss rate is given by

$$v_0 = \frac{1}{N_e(0)}\left.\frac{dN_e}{dt}\right|_{t=0}. \tag{5}$$

This is the initial slope of the $N_e(t)/N_e(0)$ curve, indicated in Fig. 4,*b* as the dotted line. We refer to v_0 as the initial rate hereafter. The measured v_0 values at various temperatures are plotted in Fig. 5 as a function of $1/T$.

The difference between the circles and the squares is the amount of H atoms fed at $t = 0$. The circles and the squares correspond to 50 and 30 discharge pulses, respectively. In the temperature range, $1/T \lesssim 3$ K^{-1}, v_0 is the ex-

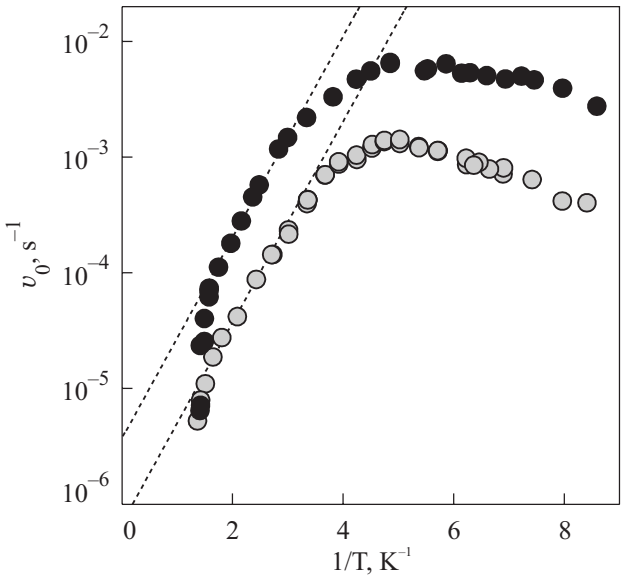

Fig. 5. Temperature dependence of the initial rate v_0. Black and gray circles denote the data for 50 and 30 discharge pulses, respectively. The dashed lines are proportional to $\exp(2E_a / k_B T)$.

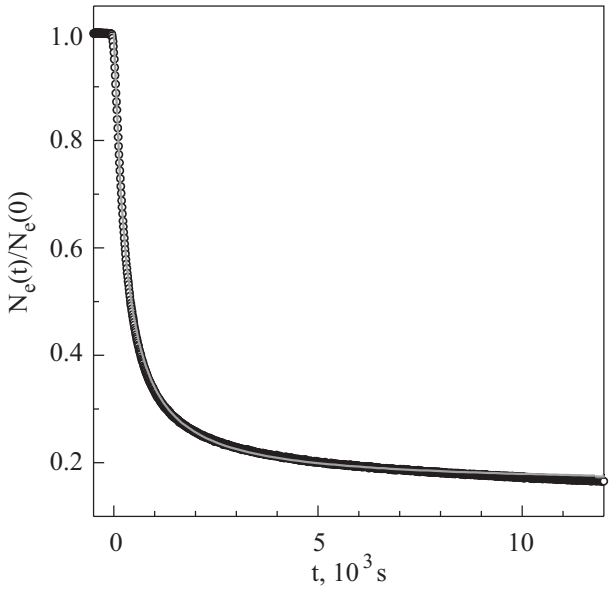

Fig. 6. Measured SSE density decay at $T = 0.33$ K (circles) and its fit to the solution Eq. (7) of the rate equation (solid line).

ponential function of $1/T$. The dashed lines in Fig. 5 are proportional to $\exp(2E_a / k_B T)$ and these lines fit the data well in $1.5\ \mathrm{K}^{-1} < 1/T < 3\ \mathrm{K}^{-1}$.

From Eq. (2), v_0 is expressed as

$$v_0 = -K_e(\alpha N_{\mathrm{H}}(0))^n. \tag{6}$$

Since the temperature dependence of K_e is weak (this will be verified later), the temperature dependence of v_0 should be dominated by α^n. At high temperatures where the second term in the bracket of Eq. (4) dominates, $\alpha \simeq (\lambda_{\mathrm{th}} / V)\exp(E_a / k_B T)$. Ignoring the $T^{-1/2}$ dependence of λ_{th}, v_0 should be proportional to $\exp(nE_a / k_B T)$. Therefore, we conclude that $n = 2$. This means that two H atoms participate in the electron attachment to form negative hydrogen, that is, the reaction $\mathrm{H} + \mathrm{H} + \mathrm{e}^- \rightarrow \mathrm{H}^- + \mathrm{H}$ is occurring in our system.

Below 0.33 K ($1/T > 3\ \mathrm{K}^{-1}$), v_0 starts to saturate or even decreases as temperature decreases. This behavior is qualitatively consistent with the temperature dependence of α. As can be seen from Eq. (4), α approaches the constant value A^{-1} at low temperatures. For our cell geometry, however, $A = 116\ \mathrm{cm}^2$ and $V = 25\ \mathrm{cm}^3$, and the crossover from the exponential temperature dependence to the constant value is expected to be at approximately 0.06 K ($1/T \approx 15\ \mathrm{K}^{-1}$), which is five times lower than 0.33 K. Unless we assume either an unrealistic surface area of the cell walls or a different temperature on the surface from the bulk liquid He, no plausible explanation has been determined yet. One of the possibilities that we cannot exclude is heating of the surface due to H recombination energy. It is said that weakness of ripplon-phonon coupling in ^{4}He is the bottleneck of cooling mechanism [18]. In this respect, the experiment on ^{3}He is worthwhile because ^{3}He can carry the heat from the surface more efficiently than ^{4}He.

In the following discussion, we focus our attention on the temperature range of $1.5\ \mathrm{K}^{-1} < 1/T < 3.0\ \mathrm{K}^{-1}$, where $v_0 \propto \exp(2E_a / k_B T)$. Putting $n = 2$ in Eq. (2) and neglecting the first term of Eq. (3), we can solve Eqs. (2)–(4) analytically to obtain

$$\frac{N_e(t)}{N_e(0)} = \exp\left[-\frac{K_e \alpha^2 N_{\mathrm{H}}^2(0) t}{K_s^{\mathrm{eff}} \alpha^2 N_{\mathrm{H}}(0) t + 1}\right]. \tag{7}$$

By fitting the measured decay curves to Eq. (7), we obtain two fitting parameters, $N_{\mathrm{H}}(0)$ and K_e. We obtained the value of K_s^{eff} from Arai *et al*. [19]. As shown in Fig. 6, Eq. (7) fits the data well.

The parameters thus obtained are $N_{\mathrm{H}}(0) = (8 \pm 1)\cdot 10^{12}$ atoms and $(3.5 \pm 0.5)\cdot 10^{12}$ atoms for the circles and the squares in Fig. 5, respectively, and $K_e = (5 \pm 3)\cdot 10^{-16}$ cm^4/s for both circles and squares. No significant temperature dependence is found for $N_{\mathrm{H}}(0)$ and K_e within our resolution.

Measurements in applied magnetic filed

When the electron spin of H atoms is polarized in strong magnetic field, H-H recombination rate is known to be suppressed [6]. It is because electronic state of bound H_2 molecule is spin singlet and thus spin triplet pair of H atoms does not proceed to H_2 unless spin flip takes place during the collision.

Likewise one can expect that electron attachment to H atom is suppressed by magnetic field since electronic spin state of H^- is singlet. In this section we show our results of electron attachment reaction rate measurements in applied magnetic fields.

Magnetic field is applied by a superconducting magnet up to 12 T. The liquid level in the sample cell is adjusted so that it coincides with the magnet center. As in the zero-field experiments, H atoms are introduced into the sample cell where SSE is prepared in advance. Since we found that the SSE loss rate is strongly suppressed in magnetic field, we kept filling H atoms at constant flux ϕ (atoms/s) in order to make the SSE loss rate faster by increasing H density in the sample cell and collide with SSE more frequently. In this case the ϕ term is added to the rate equation for $N_{\rm H}$ as

$$\frac{dN_{\rm H}}{dt} = \phi - K_e N_e (\alpha N_{\rm H})^2 - K_s^{\rm eff} (\alpha N_{\rm H})^2. \qquad (8)$$

Like the zero-field data, we recognized the same scaling behavior of the SSE loss curves at all magnetic fields. Accordingly, we may ignore the electron attachment term in Eq. (8).

The solution of the coupled rate equations including ϕ is given by

$$N_{\rm H}(t) = \frac{\phi}{q} \tanh(qt) \qquad (9)$$

for $N_{\rm H}$ and

$$\frac{N_e(t)}{N_e(0)} = \exp\left[\frac{p}{q}\tanh(qt) - at\right], \qquad (10)$$

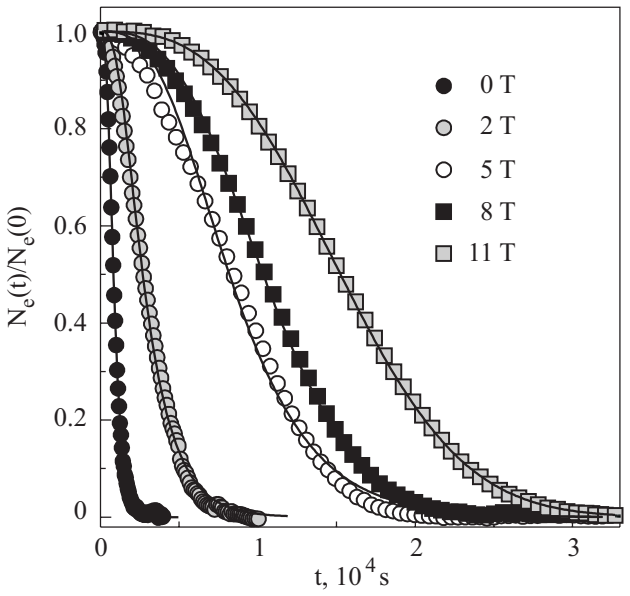

Fig. 7. Scaled SSE loss curves at few B (magnetic fields). The dots are data points and the lines are fitting results. Magnetic field suppresses the reaction and the lifetime of the two-dimensional gas mixture becomes longer.

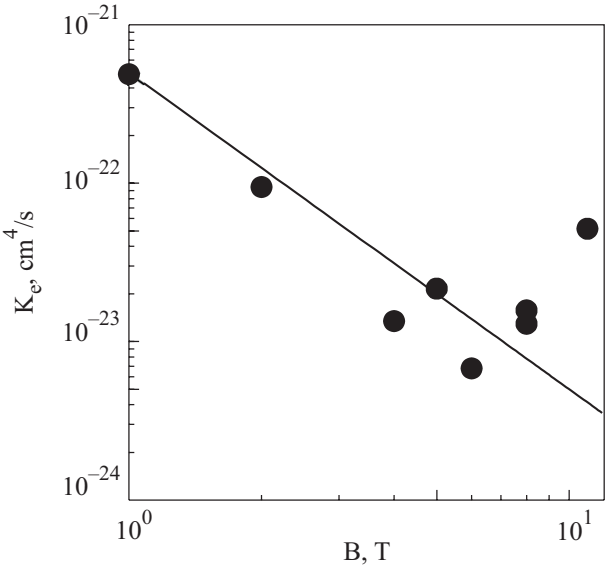

Fig. 8. Magnetic field dependence of electron attachment rate coefficient at $T = 0.3$ K. Circles are experimentally determined values and the line is drawn proportional to B^{-2}.

for N_e, where $p = K_e\phi / K_s^{\rm eff}$ and $q = \alpha\sqrt{\phi K_s^{\rm eff}}$.

Figure 7 shows scaled SSE loss curves at various magnetic fields. One can see that strong magnetic field suppresses electron attachment reaction rate. The dots are data points and the lines are fitting results to Eq. (9) with two adjustable parameters p and q. The SSE loss curves are very well fitted and hence the rate equations describe the reactions correctly. The fitting results give $\phi = (2 \pm 1)\cdot 10^{12}$ atoms/s for $B = 0.2$ T and K_e shown as dots in Fig. 8. The line in the Fig. 8 is in proportion to B^{-2}. The data shows that $K_e \sim B^{-2}$. We will discuss this point in the next section.

Discussion

We discuss here two possible microscopic mechanisms of the reaction: direct three-body collision process and dissociative attachment (DA) process. Our result $n = 2$ is reasonable because the cross section of radiative attachment $H + e^- \to H^- + h\nu$ for slow electron impact is very small and in this case a third body is required for energy conservation [20,21].

As for the direct three-body collision $H + H + e^-$, the rate coefficient, K_e, may be estimated roughly as $K_e \sim a^3 \overline{v_{\rm H}}$ from a simple consideration of collision frequency [22], where a is the scattering cross length and $\overline{v_{\rm H}}$ is the thermal velocity of H atoms. We may consider two scattering cross lengths, one is the cross length associated with the interaction between two hydrogen atoms and the other is associated with the interaction between an electron and atomic hydrogen. The former cross length might be on the order of atomic scale (10^{-8} cm), while the latter should have a much longer range because of the

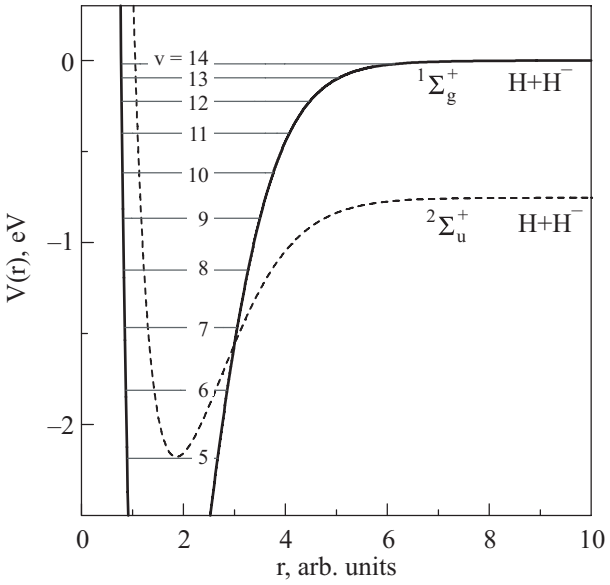

Fig. 9. The adiabatic potential curves of $^1\Sigma_g^+$ H_2 (solid line) [26] with vibrationally excited levels of $J=0$ states [27] and $^2\Sigma_u^+$ H_2^- (dashed line) [28].

charge-induced dipole moment of atomic hydrogen, which may be given by $b \approx (2\alpha_H e^2/k_B T)^{1/4}$, where $\alpha_H \approx (9/2)a_B^3$ is the polarizability of the hydrogen atom, where a_B is the Bohr radius, and e is the elementary charge. The numerical value of b amounts to $(3\sim4)\cdot10^{-7}$ cm. If we assume that a equals to b, $K_e \sim a^3\overline{v_H}$ gives a reasonable agreement with the measured value, otherwise the rate coefficient becomes too small to explain the experimental observation. It is interesting indeed to have a microscopic calculation for the direct three-body process, which should take into account the influence of the helium surface.

Another candidate is the following two-step mechanism. (i) $H+H \rightarrow H_2(v,J)$, (ii) $H_2(v,J)+e^- \rightarrow H+H^-$. The first step is the surface H recombination which is known that a rotationally and vibrationally excited molecule $H_2(14,4)$ or $H_2(14,3)$, v and J are vibrational and rotational quantum number, respectively, is produced first and it relaxes toward ground state by colliding with the sorroundings [23]. The second step is the DA of an electron to a H_2 molecule. DA reaction proceeds via the formation of H_2^- molecular anion resonance state [1]. In Fig. 9, the adiabatic potentials of $^1\Sigma_g^+$ H_2 with vibrationally excited levels of $J=0$ states and $^2\Sigma_u^+$ H_2^- are plotted. From the energy consideration, DA is possible when the total (= electronic + nuclear) energy of H_2^- is above its dissociation limit, i.e., in our case, it is necessary for $H_2(v,J)$ to capture an electron before it relaxes below the H_2^- dissociation limit since the kinetic energy of e^- on helium surface is too small to excite the molecular vibrational motion. In other words, DA which we consider now is exothermic. If $J=0$, the $H_2(v\geq10)$ states are above H_2^- dissociation limit. Exothermic DA is expected to exhibit very large cross sections at low energies [24], however, almost all the previous works are on the endothermic DA and exothermic DA is not well understood.

Applying the DA model, we have to rewrite the rate equation for N_e as

$$\frac{dN_e}{dt} = -\frac{K_{DA}}{A_e} N_* N_e, \tag{11}$$

where K_{DA} is the surface DA rate coefficient and N_* is the number of $H_2(v,J)$ in the area A_e whose energies are above the H_2^- dissociation limit. The rate equation for N_* is

$$\frac{dN_*}{dt} = \frac{1}{2}K_s A_e \alpha^2 N_H^2 - \frac{1}{\tau}N_* - \frac{K_{DA}}{A_e}N_* N_e\,. \tag{12}$$

The first term is the surface H recombination rate in A_e and the second term is the relaxation rate of $H_2(v,J)$ with its lifetime τ. If we take a steady state approximation $dN_*/dt = 0$ and assume that $N_*/\tau >> K_{DA}N_* N_e/A_e$, Eq. (11) will be

$$\frac{dN_e}{dt} = -\frac{1}{2}K_s K_{DA}\tau\alpha^2 N_e N_H^2. \tag{13}$$

Equation (13) takes the same form as Eq. (2) with $n=2$ and

$$K_e = \frac{1}{2}K_s K_{DA}\tau\,. \tag{14}$$

Therefore our analysis holds without modification. Using Eq. (14) and the measured K_e, we can roughly estimate τ. To do this we refer to a calculated maximum value of 3D endothermic DA cross section $\sigma_{DA} = 10^{-15}$ cm^2 for initial state $H_2(9,0)$ [25]. We treat our 2D gas as a squashed 3D gas of thickness d and write $K_{DA} = \sigma_{DA}\overline{v_e}/d$ where $\overline{v_e} = \sqrt{\pi k_B T/2m_e}$ is the 2D mean speed of e^-. Taking $d \sim 5$ Å, which corresponds to the thickness of H layer, we have $\tau = 10^{-9} \sim 10^{-8}$ s.

The suppression of K_e and its B^{-2} dependence can be explained as follows. For comparison with our experimental results, a line proportional to B^{-2} is drawn in Fig. 8. Since two electrons in the bound state of H^- are spin singlet, large suppression of measured K_e by magnetic field suggests that contribution from electron spin triplet collision followed by spin flip is absent or small.

If the reaction proceeds via DA, the rate determining step would be the H recombination. For our H densities, the recombination mechanism is well described in terms of van der Waals recombination [6]. The magnetic field dependence of van der Waals recombination rate coefficient is $K_s^{\text{eff}} \sim B^{-2}$ and then our measured B^{-2} dependence can be understood.

If the reaction is via direct three-body collision, we can understand the B^{-2} dependence by following the same discussion as van der Waals recombination. Electron attachment reaction rate is given by the golden rule

$$\Gamma = \frac{2\pi}{\hbar} \sum_{i,f} \left| \langle f | \hat{T} | i \rangle \right|^2 \delta(E_f - E_i), \qquad (15)$$

where i and f denote initial state $e^- + H + H$ and final state $H^- + H$, respectively. If $\hat{T}$ operator does not induce spin flip, singlet character is required for e^-–H pair to have non zero transition amplitude. In strong magnetic fields, SSE energetically favors spin down state. On the other hand, there are two high field seeking hyperfine states of H, in conventional notations, $|a\rangle = \cos\theta\,|-+\rangle - \sin\theta\,|+-\rangle$ and $|b\rangle = |--\rangle$, where $\sin\theta$ is a small coefficient proportional to $1/B$ at high field. $|+-\rangle$ denotes electron spin up and nuclear spin down, and so on. Therefore, only the $\sin\theta\,|+-\rangle$ component in $|a\rangle$ state atom gives non zero transition matrix and Γ is proportional to B^{-2} as well as hydrogen recombination rates.

Summary

We studied reaction process in two-dimensional mixture gas of electrons and hydrogen atoms bound on liquid helium surface at temperatures below 1 K. When these two species were mixed on the surface, a loss of surface charge was observed. The loss was attributed to electron attachment reaction to a H atom. We measured its reaction rates at various temperatures and magnetic fields. From the analysis of our data, we concluded that the reaction includes an electron and two H atoms: $H + H + e^- \rightarrow \rightarrow H^- + H$. Two possible mechanisms were proposed: direct three-body collision process and dissociative attachment process.

The measured suppression of the reaction rate coefficient and its B^{-2} dependence were well described by electron singlet collision.

We believe that the cryogenic electron-hydrogen system will cast a new light on the study of slow electron impact on atoms and molecules.

Acknowledgments

This work has been supported by President's Special Research Grant of RIKEN, Grant-in-Aid for Scientific Research (B) from JSPS and Grant-in-Aid for Exploratory Research from MEXT.

We thank T. Shiino and T. Mitsui for partial collaboration. We are grateful to A. Würl and P. Leiderer for VCE installation and valuable discussions. We are grateful to T. Kumada for informing us the charge-induced dipole interaction. This work was carried out under the Joint Research Program of the Institute for Solid State Physics, University of Tokyo.

1. A. Chutjian, A. Garscadden, and J.M. Wadehra, *Phys. Rep.* **264**, 393 (1996).
2. L. Sanche, *Eur. Phys. J.* **D35**, 367 (2005).
3. M.W. Cole and M.H. Cohen, *Phys. Rev. Lett.* **23**, 1238 (1969).
4. *Two-Dimensional Electron Systems on Helium and other Cryogenic Substrates*, E. Andrei (ed.), Kluwer Academic Publishers, Netherlands, (1997).
5. J.T.M. Walraven, in: *Fundamental Systems In Quantum Optics*, J. Dalibard, J.M. Raimond, and J. Zinn-Justin (eds.) (Elsevier Science Publishers B.V. (1992), p. 485.
6. I.F. Silvera and J.T.M. Walraven, in: *Prog. in Low Temp. Phys. Vol. X*, D.F. Brewer (ed.), Elsevier Science Publishers B.V., Amsterdam (1986), p. 139.
7. D.G. Fried, T.C. Killian, L. Willmann, D. Landhuis, S.C. Moss, D. Kleppner, and T.J. Greytak, *Phys. Rev. Lett.* **81**, 3811 (1998).
8. A.I. Safonov, S.A. Vasilyev, I.S. Yasnikov, I.I. Lukashevich, and S. Jaakkola, *Phys. Rev. Lett.* **81**, 4545 (1998).
9. I.F. Silvera and J.T. M. Walraven, *Phys. Rev. Lett.* **44**, 164 (1980).
10. T. Arai, T. Shiino, and K. Kono, *Physica* **E6**, 880 (2000).
11. T. Arai, A. Würl, P. Leiderer, T. Shiino, and K. Kono, *Physica* **B284-288**, 164 (2000).
12. T. Arai and K. Kono, *Physica* **B329–333**, 415 (2003).
13. M. Mertig, E. Tjukanov, S.A. Vasilyev, A.Y. Katunin, and S. Jaakkola, *J. Low Temp. Phys.* **100**, 45 (1995).
14. J.C. Collingwood and J.W. White, *J. Sci. Instrum*. **44**, 509 (1967).
15. W.N. Hardy, M. Morrow, R. Jochemsen, and A.J. Berlinsky, *Physica* **B&C110**, 1964 (1982).
16. R. van Roijen, J.J. Berkhout, S. Jaakkola, and J.T. M. Walraven, *Phys. Rev. Lett.* **61**, 931 (1988).
17. W.N. Hardy, M.D. Hürlimann, and R.W. Cline, *Jpn. J. Appl. Phys.* **26**, 2065 (1987).
18. M.W. Reynolds, I.D. Setija, and G.V. Shlyapnikov, *Phys. Rev.* **B46**, 575 (1992).
19. T. Arai, M. Yamane, A. Fukuda, and T. Mizusaki, *J. Low Temp. Phys.* **112**, 373 (1998).
20. S.J. Smith and D.S. Burch, *Phys. Rev. Lett.* **2**, 165 (1959).
21. A. Dalgarno, in: *Atomic Physics in Astrophysics*, M. Chrétien and E. Lipworth (eds.), Gordon and Breach Science Publishers (1971), p. 284.
22. *Chemical Kinetics and Reaction Mechanisms*, F. Wilkinson (ed.), Van Nostrand Reinhold Company, (1980).
23. J.M. Greben, A.W. Thomas, and A.J. Berlinsky, *Can. J. Phys.* **59**, 945 (1981).
24. I.I. Fabrikant and H. Hotop, *Phys. Rev.* **A63**, 022706 (2001).
25. Y. Xu, A.K. Kazansky, and I.I. Fabrikant, *Phys. Rev.* **A63**, 014703 (2000).
26. W. Kolos, K. Szalewicz, and H.J. Monkhorst, *J. Chem. Phys*. **84**, 3278 (1986).
27. I. Dabrowski, *Can. J. Phys*. **62**, 1639 (1984).
28. J.N. Bardsley and J.M. Wadehra, *Phys. Rev.* **A20**, 1398 (1979).